Teknomekanik, Vol. 9, No. 1, pp. 60-76, February 2026
e-ISSN: 2621-8720 p-ISSN: 2621-9980

Spatial modelling of shallow groundwater quality in coastal areas with Kriging interpolation

Yaumal Arbi[1*], Nurhasan Syah[2], Iswandi Umar[3], Indang Dewata[4], Mulya Gusman[5] and Nevy Sandra[2]

[1] Doctoral Program of Environmental Science, Universitas Negeri Padang, **Indonesia**
[2] Department of Civil Engineering, Faculty of Engineering, Universitas Negeri Padang, **Indonesia**
[3] Department of Geography, Universitas Negeri Padang, **Indonesia**
[4] Department of Chemistry, Universitas Negeri Padang, **Indonesia**
[5] Department of Mining Engineering, Faculty of Engineering, Universitas Negeri Padang, **Indonesia**

[*]Corresponding Author: yaumalarbi@ft.unp.ac.id
Received: 30 September 2025; *Revised:* 30 January 2026; *Accepted:* 08 February 2026

Cite this https://doi.org/10.24036/teknomekanik.v9i1.47272

Abstract: This study maps shallow coastal groundwater quality in Padang, Indonesia, using four operational parameters: potential of hydrogen (pH), electrical conductivity (EC), total dissolved solids (TDS), and salinity. We characterize spatial dependence using empirical variograms, evaluate directional anisotropy, and generate prediction surfaces with Ordinary Kriging. The variogram analysis indicates stronger spatial continuity along the coastline for EC and TDS, while salinity shows shorter continuity with a distinct directional structure, reflecting localized freshwater-seawater mixing processes. Groundwater pH remains neutral to slightly alkaline and exhibits lower spatial variability than EC, TDS, and salinity. Leave-one-out cross-validation supports the reliability of the kriging estimates at the study scale, indicating low prediction error and strong agreement between observed and predicted values. The resulting thematic maps enable a three-level quality zoning that differentiates a lower-risk northern segment, a transitional central belt, and a higher-risk southern segment consistent with seawater intrusion influence. These outputs provide a practical basis for prioritizing monitoring locations, protecting vulnerable wells, and strengthening evidence-based coastal groundwater management aligned with SDG 6 Clean Water and Sanitation and SDG 11 Sustainable Cities and Communities.

Keywords: coastal groundwater; seawater intrusion; ordinary kriging; clean water and sanitation; sustainable and communities

1. Introduction

Seawater intrusion is a major issue for shallow groundwater in coastal cities because rising freshwater demand shifts the interface between freshwater and saline water [1], [2]. Sea level rise and climate change further increase salinization risk and expand its impacts on coastal water resources. Excessive groundwater abstraction driven by population growth and economic activity accelerates intrusion and can reduce water quality beyond levels suitable for domestic use and irrigation [3], [4]. Coastal development in Padang increases the vulnerability of shallow aquifers, so monitoring groundwater characteristics becomes essential to protect local water security [5]. Mapping and monitoring the freshwater–seawater mixing zone help managers assess disturbance levels and target mitigation actions more precisely in the field [6].

Field studies along the Padang coast commonly assess seawater intrusion indicators by measuring electrical conductivity and salinity in shallow dug wells, with an emphasis on these as rapid screening parameters [7], [8]. Studies in the Padang Barat area report spatial variation in electrical conductivity and salinity across observation points and interpret intrusion tendencies using value classes and

proximity to the shoreline[9]. Other work in the coastal zone of Padang maps groundwater levels and salinity zoning and highlights seasonal differences as a control on changes in shallow groundwater salinity [10]. In other Indonesian coastal settings, GIS-based studies use combinations of electrical conductivity, total dissolved solids, and salinity to describe intrusion patterns, but many analyses remain descriptive and do not quantify spatial dependence. Several studies apply distance-based interpolation, such as inverse distance weighting, to generate distribution maps, and some compare interpolation performance using prediction error metrics [11], [12]. Differences in spatial coverage, indicator selection, and mapping methods make it difficult to align on consistent city-scale coastal risk zoning [13].

International research increasingly adopts multi-parameter groundwater quality mapping and spatial clustering to support more adaptive monitoring and management strategies[14]. Method calibration has also advanced, since comparative studies often show kriging performs better than deterministic interpolation, while performance depends strongly on variogram selection and correct representation of spatial structure [15]. In hydrogeology, researchers frequently use leave-one-out cross-validation to select the most suitable spatial model and to evaluate kriging accuracy before using maps for decision-making. In coastal aquifers, intrusion dynamics can extend along the shoreline and respond to heterogeneity and pumping, so models that ignore directional continuity may blur salinization signals and mixing-zone boundaries [16], [17]. Geostatistical literature treats the semivariogram as the core of estimation because parameters such as nugget, sill, and range control continuity patterns, yet some applied studies emphasize final maps without sufficient reporting of variogram structure and testing [18], [19]. These limitations highlight the need for multi-parameter mapping that explicitly tests coastal anisotropy and reports prediction validation to strengthen zoning for monitoring prioritization and well protection [19], [20].

This study aims to map shallow coastal groundwater quality in Padang using four operational parameters: potential of hydrogen (pH), electrical conductivity (EC), total dissolved solids (TDS), and salinity. The study builds variogram models for each parameter, tests for anisotropy to ensure alongshore and cross-shore continuity are represented, and produces prediction surfaces using Ordinary Kriging. The study evaluates mapping reliability using leave-one-out cross-validation, providing maps with a clear accuracy basis for managerial use. The study then derives a three-level quality zoning to distinguish coastal segments with lower risk, transitional conditions, and higher risk related to salinization indicators. The outputs support SDG 6 Clean Water and Sanitation by enabling more targeted groundwater quality monitoring, and they also relate to SDG 11 Sustainable Cities and Communities by helping the city manage coastal environmental risks and protect water sources for settlements.

2. Material and methods

2.1 Study location

The study area lies along the coastal corridor of Padang City, West Sumatra, which is characterized by a narrow coastal plain bordering the Indian Ocean and a rapid transition eastward into hills and the Barisan Mountains. Coastal alluvial deposits dominated by sand, silt, and clay form a shallow unconfined aquifer that generally extends parallel to the shoreline and interacts with the local hydrologic system. Major river systems, particularly Batang Arau, Batang Kuranji, and their tributaries, create estuarine transition zones that can influence freshwater–saline water mixing within the shallow aquifer [21]. Land use along this corridor is dominated by urban settlements, commercial and service activities, port facilities, and small to medium industrial clusters along coastal transport routes, which increases anthropogenic pressure on groundwater quality. Daily tidal dynamics, seasonal runoff, and local groundwater abstraction interact with these geological

and hydrological conditions and contribute to spatial variability in groundwater quality from nearshore areas to several kilometers inland [22].

This study compiled administrative layers and observation points using Padang's operational base map and distributed observation locations along the northern-to-southern segments of the coastal corridor, extending into the inland transition zone to capture the coastal-to-inland gradient. Coordinates for each point were recorded in a geographic coordinate system referenced to the WGS 84 datum, and all geostatistical processing was carried out in a Universal Transverse Mercator projection covering the Padang region so that distance and anisotropy directions were computed in meters. This procedure ensured spatial consistency for variogram modeling, anisotropy testing, and Ordinary Kriging interpolation, while reducing bias associated with coordinate-system mismatches across layers. Each observation point includes field measurements of pH, electrical conductivity, total dissolved solids, and salinity, enabling interpolated maps to distinguish stable areas, transition zones, and areas with stronger salinization indicators. The sampling configuration, which spans residential zones and estuarine areas, supports hotspot identification in the resulting maps, particularly locations potentially influenced by seawater intrusion.

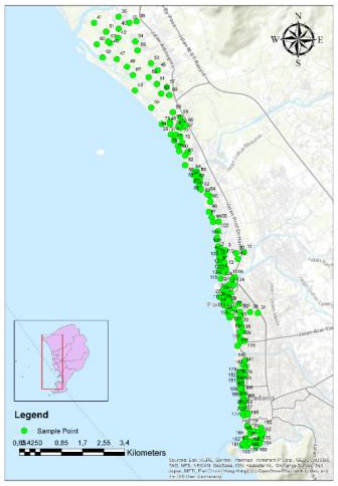

Figure 1. Sample location

2.2 Sampling period and design

Sampling was conducted from 2 September 2025 to 20 October 2025. We visited each well once and measured pH, electrical conductivity (EC), total dissolved solids (TDS), and salinity in situ at the time of sampling. We recorded site notes on coastal influence (proximity to shorelines or river mouths) to support the interpretation of EC, TDS, and salinity patterns. The dataset, therefore, represents a September–October snapshot of shallow unconfined wells along the Padang coastal corridor and the inland transition zone.

2.3 Field instruments

We measured pH using a benchtop pH meter Mettler Toledo SevenCompact S220. We measured EC, TDS, salinity, and water temperature using a portable Water Quality Meter AZ Instrument 86031, which provides automatic temperature compensation for conductivity measurements.

2.4 Calibration standards and quality control

For pH, we calibrated the S220 before daily measurements using a three-point calibration with fresh standard buffers pH 4.01, 7.00, and 10.01, then rinsed the electrode with deionized water between

buffers and samples. For EC on the AZ 86031, we calibrated the conductivity probe using certified conductivity standards that match the meter calibration points: 146.6 µS/cm, 1413 µS/cm, 12.88 mS/cm, and 51.5 mS/cm, selected based on the measurement range encountered in the field. The meter stores calibration by range, so we calibrated the relevant range used during the campaign and avoided reusing the calibration solution. For TDS, we reported the meter output using its conductivity-to-TDS conversion factor. We kept tdF at 0.50 (default setting) and report this value for reproducibility. For salinity, the AZ 86031 reports salinity in ppt, and we used the instrument's direct salinity display. At each well, we rinsed the probes with deionized water, immersed the sensor fully, gently stirred to homogenize, waited for stabilization, and then recorded the final readings. We repeated readings when values did not stabilize and used the stable reading for analysis.

2.5 Semivariogram, model and parameters

The semivariogram is a key component of kriging because it describes how similar data values (pH, EC, TDS, and salinity) are as observation points become farther apart. In this study, the data is second-order stationary, meaning that the mean is considered relatively constant on a local scale and the relationship between data points (covariance) is determined by distance and direction, not by their exact location [23], [24]. If there is a clear trend, for example, an increase or decrease in values from the coast towards the mainland, we first remove the trend (detrending). The aim is for the semivariogram to accurately reflect average fluctuations, not large-scale trends. Empirical variogram [25].

$$\hat{\gamma}(h) = \frac{1}{2N(h)} \sum_{(i,j)\in h} [[Z]](S_i) - Z(S_j)]^2 \quad (1)$$

Empirical semivariograms were computed using the Matheron estimator on coordinates projected to UTM Zone 47S (WGS 84), so all separation distances are in meters[26], [27]. We set the cutoff distance to the 90th percentile (P90) of all inter-point distances, yielding a cutoff of 16,000 m. The lag structure used 12 distance classes, giving a lag width of 1,333 m. We enforced a minimum of 20-point pairs per lag; in practice, the number of pairs per lag was typically on the order of 10^3, which supports stable empirical variogram estimation. We tested three theoretical models (Spherical, Exponential, and Gaussian) and selected the best model by minimizing the RMSE between the fitted model and the empirical semivariogram. To evaluate geometric anisotropy, we computed directional semivariograms at azimuths 0°, 45°, 90°, and 135°, with an angular tolerance of ±22.5°, and compared the directional ranges to identify the main continuity direction and the range ratio. Model selection. The three basic models tested for each parameter are Spherical, Exponential, and Gaussian [28]:

- Spherical: $\hat{\gamma}(h) = C_0 + C\left[\frac{3h}{2\alpha} - \frac{h^2}{2\alpha^3}\right]$ for $0<h\leq\alpha$; $\hat{\gamma}(h) = C_0 + C$ for $h> \alpha$. Has a definite range α where the variogram reaches the sill.
- Exponential: $\hat{\gamma}(h) = C_0 + C\left[1 \exp\left(-\frac{h}{\alpha}\right)\right]$. Never truly reaches the sill; practical range $\approx 3\alpha$
- Gaussian: $\hat{\gamma}(h) = C_0 + C\left[1 \exp\left(-\frac{h^2}{\alpha^2}\right)\right]$. Very smooth, close to the origin; practical range$\approx \sqrt{3\alpha}$

Parameter nugget, sill, range.

- Nugget (C_0) represents very small-scale variability or measurement error; a large nugget indicates high irregularity.

- Sill total ($C_0 + C$) approximates the overall variability of the process on a large scale; the partial sill C is spatially structured variability.
- Range (α) s a measure of continuity; point pairs that are further apart from the range become almost uncorrelated.

Ordinary Kriging (OK) is used as the primary interpolation method to generate estimates of groundwater quality parameters (pH, EC, TDS, salinity) at unmeasured locations with unbiased estimators and minimum variance [29]. OK assumes a constant but unknown local mean around the estimation location; this assumption is realistic for shallow coastal aquifers, while spatial continuity is used by the selected semivariogram model [30]. Operationally, the value at the target position S_0 is calculated as a weighted combination of surrounding observations using Equation 2.

$$\hat{Z}(S_0) = \sum_{i-1}^{n} \lambda_i \, Z\,(S_i) \tag{2}$$

With unbiased constraints $\sum_{i-1}^{n} \lambda_i$ =1. The weights λ_i are obtained by minimizing the kriging error variance $\sigma_K^2 = Var\left\{\hat{Z}(S_0) - Z(S_0)\right\}$ using the Lagrange multiplier μ, so that they satisfy the system of linear Equation 3.

$$\begin{bmatrix} \gamma(S_1,S_1) & \cdots & \gamma(S_1,S_n) & 1 \\ \vdots & \ddots & \vdots & \vdots \\ \gamma(S_n,S_1) & \cdots & \gamma(S_n,S_n) & 1 \\ 1 & \cdots & 1 & 0 \end{bmatrix} \begin{bmatrix} \lambda_1 \\ \vdots \\ \lambda_n \\ \mu \end{bmatrix} = \begin{bmatrix} \gamma(S_1,S_0) \\ \vdots \\ \gamma(S_n,S_0) \\ 1 \end{bmatrix} \tag{3}$$

$\gamma(S_i,S_j)$ is a structured semivariogram evaluated from the model (spherical/exponential/gaussian) at distances and directions between points. After the weights and μ are obtained, the kriging variance at location S_0 is calculated using Equation 4.

$$\sigma_K^2(S_0) = \sum_{i-1}^{n} \lambda_i \, \gamma\,(S_i\,, S_0) + \mu \tag{4}$$

Water quality mapping generally uses variograms directly because they are closely related to the estimated nugget, sill, and range parameters. In coastal environments such as Padang, the possibility of geometric anisotropy (continuity in directions parallel vs. perpendicular to the coast) is addressed using an anisotropic variogram or coordinate rescaling, so that the effective distance accounts for the main direction and anisotropy ratio. To avoid unstable matrices, the search neighbourhood is generally set sectorally and the maximum radius is close to the practical range, so that the weights are not dominated by a single direction.

2.6 Kriging neighborhood and grid settings

We generated prediction rasters using a fixed 100 m grid for all parameters. We applied a sector-based search neighborhood (4 sectors) to reduce clustering effects and to stabilize the kriging system under anisotropy. We set the search radius to match the practical range of each fitted variogram, namely 3,843 m for pH, 4,064 m for EC, 3,999 m for TDS, and 1,383 m for salinity. We set the minimum number of neighbors to 5 and the maximum to 15, and required at least one neighbor per sector when available. We used the same neighborhood settings for both map generation and leave-one-out cross-validation to keep validation consistent with the mapping configuration. We tested the sensitivity of the neighborhood configuration by varying the maximum neighbors (15 to 20) and the search radius (0.8× to 1.2× the practical range). The predicted spatial patterns and cross-validation metrics remained stable, so we retained the settings reported above for all final maps.

2.7 Cross validation, RMSE, and R^2

To assess the reliability of the Ordinary Kriging results map, this study applied leave-one-out cross-validation. In principle, each observation $Z(S_i)$ s sequentially removed from the data set, then predicted again at its own location using all other points and the same variogram model as in mapping. The prediction at the location S_i is expressed in Equation 5.

$$\hat{Z}^{(-i)}(S_i) = \sum_{j \neq i} \lambda_{ij} Z(S_j) \quad (5)$$

with weights λ_{ij} obtained from the kriging system that does not include point i. The difference between the observation and the LOOCV prediction is defined as the residual in Equation 6.

$$r_i = Z(si) - \hat{Z}^{(-i)}(S_i) \quad (6)$$

The main accuracy measure reported is Root Mean Square Error (RMSE), which summarizes the average square errors in the variables Equation 7.

$$\text{RMSE} = \sqrt{\frac{1}{n}\sum_{i=1}^{n} r_i^2} \quad (7)$$

Overall performance was also evaluated using the LOOCV-based coefficient of determination using equation 8.

$$R^2 = 1 - \frac{\sum_{i=1}^{n}(Z(S_i) - \hat{Z}^{(-i)}(S_i))^2}{\sum_{i=1}^{n}(Z(S_i) - \hat{Z})^2} \quad (8)$$

The R^2 value is in the range [0,1]; the closer it is to 1, the greater the proportion of variation in the observations that can be explained by the kriging model being tested.

As a basis for quality classification on the results map, this study adopted standard drinking water quality criteria referenced from SNI and WHO for the parameters measured; for pH, the acceptable operational range is 6.5–8.5 as recommended in national and international guidelines; for TDS, Indonesian national standards set a limit of 500 mg/L as the recommended threshold value for drinking water, while the WHO does not provide specific health-based guideline values for TDS but emphasizes that the taste of water is generally still acceptable up to around 600 mg/L; for EC, neither SNI nor WHO sets a direct health threshold, and EC is generally used as an operational indicator correlated with dissolved ions; while salinity is not given a specific health threshold value by either the SNI, so its assessment in this study was carried out indicatively through a combination of EC, TDS. We summarize LOOCV performance using Mean Error (ME) to indicate bias, Root-Mean-Square Error (RMSE) to indicate average prediction error magnitude, and Root-Mean-Square Standardized Error (RMSSE) to evaluate error calibration. We also report the LOOCV-based coefficient of determination (R^2) to indicate explained variance.

3. Results and discussion

Based on 207 observation points, the basic characteristics of shallow coastal groundwater quality in Padang show a pattern consistent with heterogeneous coastal aquifers. The pH value is relatively stable, while EC, TDS, and salinity exhibit greater variation. The average TDS ≈ 508 mg/L is around the threshold of 500 mg/L in the Indonesian National Standard for drinking water (operational indicator), and EC is used as an operational indicator without assuming a single linear conversion. Figure 2 shows that the pH of groundwater ranges from 6.0 to >8.0 (generally neutral to slightly alkaline); EC varies widely from 92 µS/cm to 3004 µS/cm; TDS from 46 mg/L to 1711

mg/L; and salinity from 0.01 ppt to 0.80 ppt. Extreme values of EC – TDS – salinity tend to occur in the central coastal segment closer to the coastline, while relatively lower values are found at points further inland. In contrast, pH is relatively stable in the neutral–weakly alkaline range, with variations attributed to aquifer mineralogy, biological activity, and mixing of local surface water and groundwater. This range pattern serves as the basis for semivariogram modeling and kriging interpolation for the pH, EC, TDS, and salinity parameters.

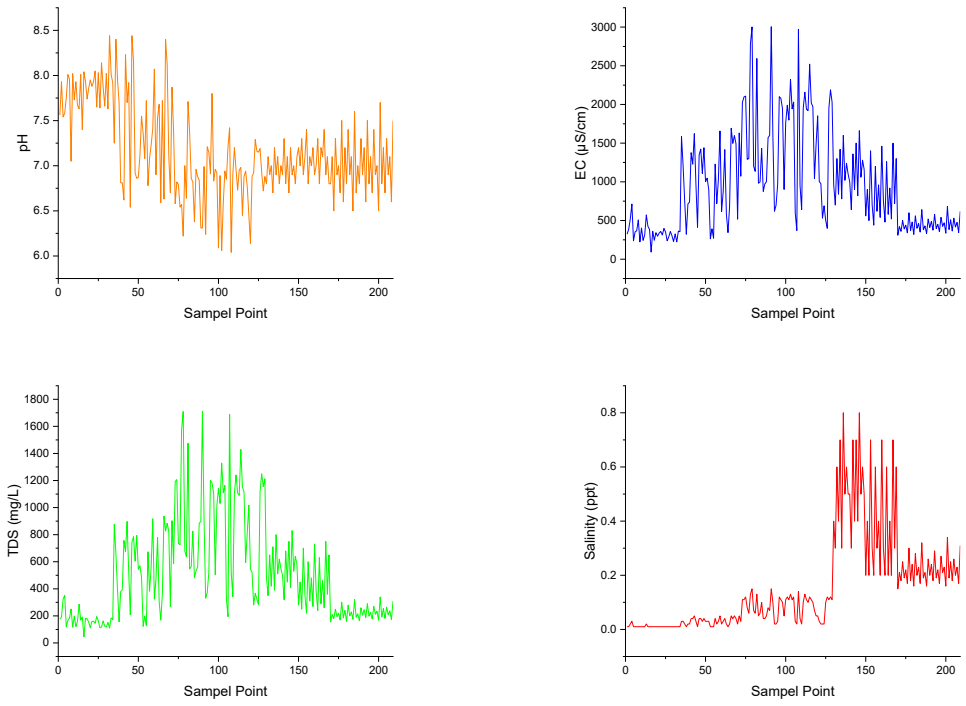

Figure 2. Results of pH, EC, TDS, and salinity measurements

Table 1. Statistics on shallow coastal groundwater parameters

Parameter	n	Mean	SD	Min	Max	CV (%)
pH	207	7.16	0.51	6.04	8.44	7.07
EC (µS/cm)	207	944.13	641.67	92.00	3004.00	67.96
TDS (mg/L)	207	508.07	370.92	46.00	1711.00	73.01
Salinity (ppt)	207	0.16	0.18	0.01	0.80	114.76

3.1 Cross-validation

We evaluated model performance using leave-one-out cross-validation (LOOCV). Mean Error (ME) close to zero indicates low bias, RMSE represents the average magnitude of prediction error, and RMSSE evaluates error calibration. Table 2 summarizes these metrics for pH, EC, TDS, and salinity and shows consistent performance across parameters for the study scale.

Table 2. LOOCV cross-validation metrics for Ordinary Kriging models

Parameter	ME	RMSE	RMSSE	R^2
pH	0.0000286	0.0127410	0.4520356	0.999373
EC (µS/cm)	1.2626850	24.9654600	0.4509394	0.998479
TDS (mg/L)	0.9298039	14.9672600	0.4246729	0.998364
Salinity (ppt)	0.0002909	0.0049641	0.4357585	0.999236

3.2 Variogram

Variogram analysis was performed on four water quality parameters (pH, EC, TDS, and salinity) using the Matheron estimator on projected coordinates in UTM Zone 47S (WGS 84), with distance units in meters. To ensure the reliability of the results, distance (lag) classes were determined robustly using a distance limit at the 90th percentile (P90), 12 classes (bins), and at least 20 pairs per class. Three theoretical models, Spherical, Exponential, and Gaussian, were tested, and the optimal model was determined based on the smallest root mean square error (RMSE) value against the empirical variogram. Anisotropy tests were conducted at azimuths of 0°, 45°, 90°, and 135°, with a tolerance of ±22.5°, to examine range differences by direction. The variogram shows a clear spatial structure for all four parameters, with the dominant range being on the order of kilometres. The ratio of nugget to sill provides an indication of the contribution of very fine-scale variability and/or measurement error, while the range indicates the scale of spatial autocorrelation of the parameter in question.

3.3 pH

The best model for pH is Spherical, with the following parameters: nugget = 0.192, sill (total) = 0.263, range = 3,843 m (3.84 km), and RMSE = 0.012. The proportion of nugget to sill of ~73% indicates a relatively large contribution from micro-scale variability/measurement error, but there is still an increase in semivariance towards the sill, so the spatial structure remains readable. The anisotropy test indicates very strong anisotropy (range ratio ≈ 157) with a main direction of ±0°.

3.4 EC

For EC, the best model is Gaussian with nugget ≈ 334.970, sill (total) ≈ 497,227, range ≈ 4,064 m (4.06 km), and RMSE ≈ 24.965. The nugget proportion ≈ 67% indicates that very-fine-scale variability is quite dominant. Anisotropy is also evident (range ratio ≈ 66), with the main direction ±0°.

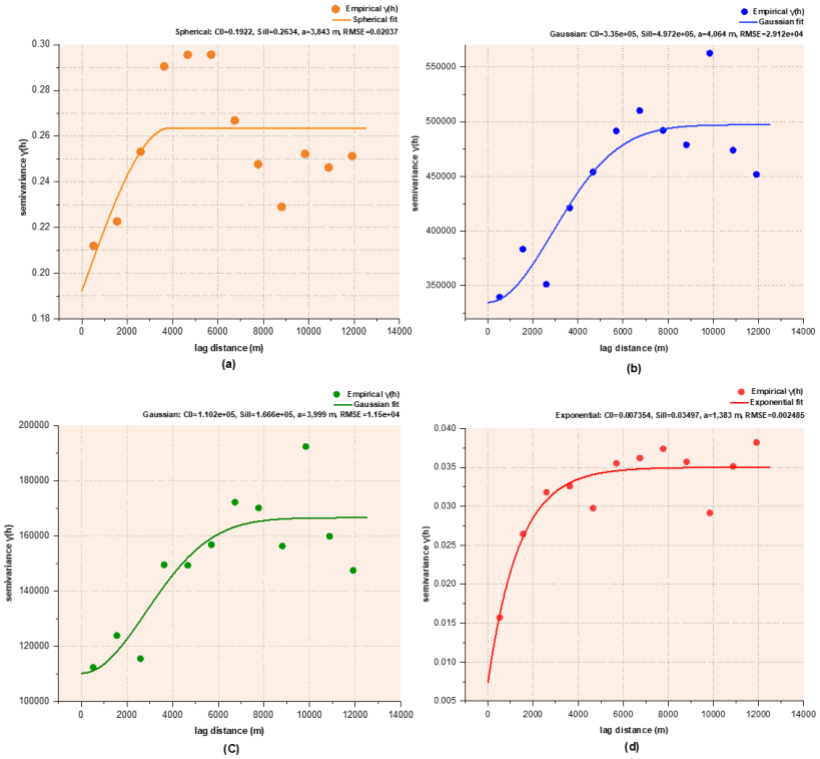

Figure 3. Variogram (a) pH, (b) EC, (c) TDS, (d) Salinity

3.5 DS

The TDS parameter is best represented by a Gaussian model, with a nugget ≈ of 110.231, sill (total) ≈ of 166.647, range ≈ of 3,999 m (≈4.00 km), and RMSE ≈ of 14.967. The nugget proportion ≈ 66% indicates a significant contribution from very-fine-scale variability. The anisotropy test shows very strong anisotropy (range ratio ≈ 281) with a principal direction of ±0°.

3.6 Salinity

For salinity, the best model is Exponential, with nugget ≈ 0.00735, sill (total) ≈ 0.03497, range ≈ 1,383 m (≈1.38 km), and RMSE ≈ 0.004. The nugget proportion ~21% indicates a relatively "cleaner" spatial structure compared to the other three parameters. Anisotropy is identified with a range ratio ≈ of 10.9 and a main direction of ±135°.

3.7 Spatial distribution of pH

The pH map indicates a neutral to slightly alkaline condition across the coastal corridor, with predicted values ranging from 6.758 to 7.631. The surface shows an elongated pattern broadly parallel to the coastline, which aligns with the directional continuity identified in the variogram analysis. This pattern suggests that pH varies more gradually along the coast than across it, while local departures likely reflect site-specific mixing conditions near rivers, drainage outlets, and coastal settlements. Spatially, pH exhibits a smaller contrast than EC, TDS, and salinity. This behavior supports the role of pH as a supporting indicator of acid–base stability rather than the primary driver of the dissolved-salt signal. Therefore, interpretation of coastal risk relies more strongly on EC, TDS, and salinity patterns, while pH helps confirm the absence of strong acidification anomalies.

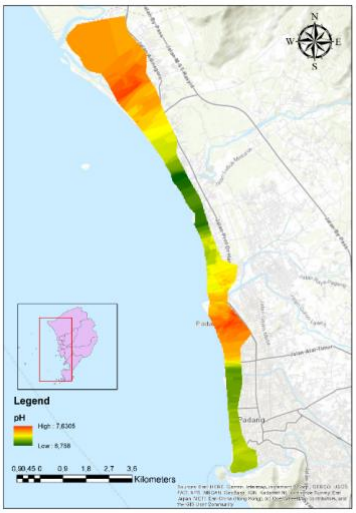

Figure 4. Spatial distribution of pH predicted by Ordinary Kriging

3.8 Spatial distribution of EC

The EC map shows predicted values ranging from 400 to 1,861 µS/cm. Higher EC zones concentrate mainly in the central to northern segment of the corridor, while lower values dominate the southern part. The surface forms a corridor-like pattern along the coastline, consistent with the anisotropic structure reported by the variogram analysis. Hydrogeochemically, elevated EC indicates higher dissolved-ion content and can reflect seawater mixing, ion enrichment near estuaries, or concentrated human inputs in densely used coastal areas. The observed along-coast

continuity supports interpretation at the corridor scale, while sharper cross-shore changes indicate stronger local gradients perpendicular to the shoreline.

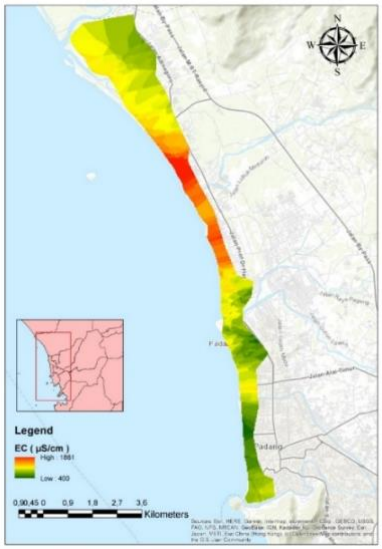

Figure 5. Spatial distribution of electrical conductivity, EC (µS/cm) predicted by Ordinary Kriging

3.9 Spatial distribution of TDS

The TDS map ranges from 197 to 1,016 mg/L and shows a spatial pattern that closely follows the EC surface. Higher TDS zones appear mainly in the central to northern segment, while lower values dominate the southern segment. This agreement supports the interpretation that EC and TDS capture a similar dissolved-salt pressure signal in the study area. The corridor-like distribution also matches the variogram results that indicate stronger continuity along the coastline than across it. This behavior suggests that regional coastal processes shape broad TDS patterns, while local inputs and hydrogeologic heterogeneity produce sharper changes over shorter cross-shore distances.

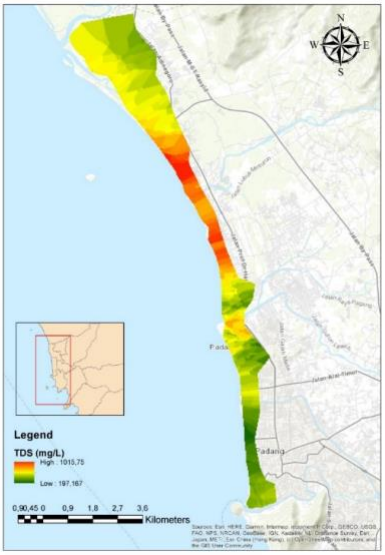

Figure 6. Spatial distribution of total dissolved solids, TDS (mg/L) predicted by Ordinary Kriging

3.10 Spatial distribution of salinity

Salinity values range from 0.02 to 0.52 ppt, with higher zones concentrated in the southern segment and decreasing toward the north. This pattern differs from EC and TDS in its hotspot location, which suggests that local mixing conditions and coastal hydrodynamics influence salinity more strongly in specific segments. The salinity surface also shows a shorter spatial scale of change than the other parameters, consistent with the shorter variogram range. Hydro-oceanographic drivers can include tidal exchange, estuary dynamics, shoreline morphology, and localized pathways of seawater intrusion. Because salinity changes over short distances, sample density becomes more important for capturing local features near high-gradient zones, such as river mouths and active coastal drainage outlets.

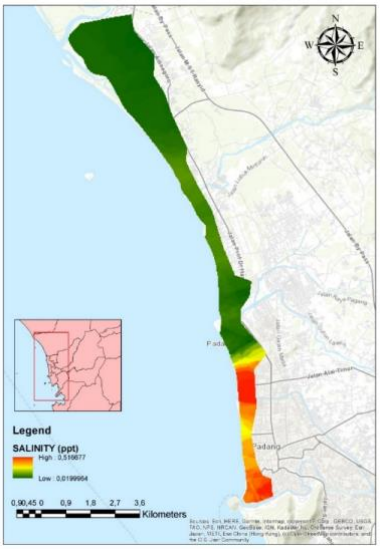

Figure 7. Spatial distribution of salinity (ppt) predicted by Ordinary Kriging

3.11 Validation note

LOOCV results indicate low bias and stable prediction performance for all four parameters at the study scale. Insert Table 2 immediately before the "Variogram" subsection, then refer to it here once to support the reliability of Figures 4–7.

3.12 Quality zoning and risk areas

We derived the quality zoning map from the four Ordinary Kriging prediction rasters (pH, EC, TDS, and salinity). We classified each raster into three classes using tertile thresholds computed from the raster value distribution (33rd and 66th percentiles), so the zoning reflects relative spatial risk within the study area. For EC, TDS, and salinity, higher values indicate higher dissolved-salt pressure, so we defined Class 1 as good (low), Class 2 as moderate, and Class 3 as low quality (high). For pH, we treated the neutral-to-slightly alkaline range as supportive of stability, so pH served as a supporting indicator rather than the primary driver of risk. In this study, the "stable" pH class is the middle tertile, defined by $7.19 < pH < 7.41$.

We built the composite zone using a rule-based approach focused on the three salt-related indicators (EC, TDS, salinity). For each grid cell, we assigned a primary score as the median of the EC, TDS, and salinity classes (median of three classes avoids bias from one extreme surface). We then used pH only as a tie-breaker when the three primary indicators produced an unstable combination (Class 1, 2, and 3 simultaneously). In that case, we assigned the cell to Class 2 (moderate) by default, and

shifted it to Class 1 only when pH fell in the "stable" class (7.19 < pH < 7.41), otherwise we kept Class 2. This procedure produces three final zones: good quality (low risk), moderate quality (transition), and low quality (high risk), and it avoids subjective visual grouping.

Table 3. Class thresholds used for zoning

Parameter	Class 1 (good)	Class 2 (moderate)	Class 3 (low)
pH	≤ 7.19	7.19 < pH < 7.41	≥ 7.41
EC (µS/cm)	≤ 835.50	835.50 < EC < 1021.17	≥ 1021.17
TDS (mg/L)	≤ 453.92	453.92 < TDS < 558.08	≥ 558.08
Salinity (ppt)	≤ 0.03083	0.03083 < Salinity < 0.06363	≥ 0.06363

3.13 Comparison with previous studies

The geostatistical literature on coastal aquifers shows that groundwater salinity mapping should represent spatial dependence so that the outputs do more than depict patterns and instead provide a testable basis for decision-making [31], [32], [33]. Established research practice treats semivariogram model selection as a key step prior to interpolation because the semivariogram controls continuity structure and estimation accuracy. Many studies also combine Ordinary Kriging with prediction assessment, making the resulting maps more transparent and reproducible [34], [35]. This framework aligns with the approach adopted in this study, which first models spatial structure and then derives zoning from evaluated interpolated surfaces.

Evidence from multiple coastal aquifers indicates that dissolved-salt indicators often form spatial patterns that follow coastal configuration and local groundwater flow conditions [36]. Kriging-based salinity mapping studies likewise emphasize the need to test spatial structure so that interpolation does not become overly smooth and does not obscure zone boundaries that matter for management [37]. Comparable examples from Indonesia show that geostatistical mapping can use physicochemical parameters such as electrical conductivity and total dissolved solids to infer intrusion signals from their spatial distributions [38]. The findings of this study fit within the same general framework while emphasizing Padang's local controls, including estuarine influences, pumping, and shallow-aquifer heterogeneity.

In Indonesian research, dug-well-based coastal studies in Padang commonly use electrical conductivity and salinity as indicators of intrusion, but their main outputs often remain point-based interpretations within limited coastal corridors[39]. Process-oriented work in Padang has also advanced through stable-isotope approaches that reveal variation in shallow groundwater characteristics and diverse recharge sources, reinforcing the need for robust maps that connect process evidence with spatial evidence. A relevant national comparison is provided by geostatistical intrusion mapping in the Jember coastal area, which uses physicochemical parameters to map salinity and infer intrusion at an administrative scale [33]. Compared with many studies that emphasize a single indicator, this study advances a consistent multi-parameter kriging framework, explicitly tests spatial structure, and delivers a more operational zoning to support monitoring prioritization and well protection.

4. Conclusion

This study developed shallow coastal groundwater quality maps for Padang City using potential of hydrogen (pH), electrical conductivity (EC), total dissolved solids (TDS), and salinity through Ordinary Kriging. Variogram analysis revealed parameter-specific spatial structures and confirmed the importance of directional continuity, particularly for indicators that are sensitive to seawater intrusion. Anisotropy testing enabled the model to capture coastal-aligned distribution patterns,

preventing the maps from over-smoothing locally important variability. Leave-one-out cross-validation indicated that the kriging models produced consistent predictions at the study scale, supporting their use as an operational basis for zoning. The resulting three-level zoning distinguishes lower-risk coastal segments, a transition zone, and higher-risk segments associated with salinization indicators. The results have direct management relevance because the multi-parameter maps support prioritization of monitoring locations, well protection, and targeted coastal interventions. Local authorities can use zoning to guide routine inspections, regulate groundwater abstraction in vulnerable areas, and plan alternative water supplies in areas with declining water quality. The multi-parameter approach also strengthens interpretation compared with single-indicator mapping, as salinity, electrical conductivity, and total dissolved solids provide complementary evidence for assessing intrusion signals. Future work should incorporate seasonal sampling, well-depth information, and hydrodynamic variables such as groundwater level and distance to the shoreline to better represent coastal dynamics. These improvements will further strengthen the contribution to SDG 6 Clean Water and Sanitation and SDG 11 Sustainable Cities and Communities through evidence-based monitoring and management of coastal groundwater.

Author's declaration

Author contribution

Yaumal Arbi: Conceptualization, Data curation, Formal analysis, Investigation, Methodology, Validation, Writing – original draft**. Nurhasan Syah:** Conceptualization, Formal analysis. **Iswandi Umar:** Formal analysis, Methodology. **Indang Dewata**: Supervision, Validation. **Mulya Gusman:** Supervision, Validation. **Nevy Sandra**: Validation.

Funding statement

This research was funded by the Government of Indonesia through the Doctoral Completion Scholarship, administered by the Pusat Pembiayaan dan Asesmen Pendidikan Tinggi (PPAPT), Kementerian Pendidikan Tinggi, Sains, dan Teknologi, and supported through Indonesia Endowment Fund for Education Agency (LPDP -*Lembaga Pengelola Dana Pendidikan*).

Data availability

Data will be made available on request.

Acknowledgements

The authors gratefully acknowledge the Government of Indonesia for support through the Doctoral Completion Scholarship. The authors also thank Universitas Negeri Padang for institutional support and facilities that enabled this research.

Competing interest

The authors declare that they have no known competing financial interests or personal relationships that could have influenced the work reported in this paper.

Ethical clearance

This research does not involve humans or animals as subjects, so an ethical document is not required.

AI statement

The grammatical structure of this article was improved by using ChatGPT, and the authors have rechecked the accuracy and correctness of the generated sentences with the topic and data of this study. The language use in this article has been validated and verified by an English language expert, and none of the AI-generated sentences are included in this article.

Publisher's and Journal's note

Universitas Negeri Padang as the publisher, and Editor of Teknomekanik state that there is no conflict of interest towards this article publication.

References

[1] R. Fajrianto, W. Wilopo, P. A. Pranantya, and P. Laowattanabandit, "Study of seawater intrusion in the coastal alluvial aquifer, West Semarang, Central Java, Indonesia," *Journal of Degraded and Mining Lands Management*, vol. 13, no. 1, pp. 9399–9413, Jan. 2026, https://doi.org/10.15243/jdmlm.2026.131.9399

[2] Q. Su, R. D. Kambale, J. H. Tzeng, G. L. Amy, D. A. Ladner, and R. Karthikeyan, "The growing trend of saltwater intrusion and its impact on coastal agriculture: Challenges and opportunities," *Science of the Total Environment*, vol. 966. Elsevier B.V., Feb. 25, 2025. https://doi.org/10.1016/j.scitotenv.2025.178701

[3] K. L. O'Donnell *et al.*, "Saltwater intrusion and sea level rise threatens U.S. rural coastal landscapes and communities," *Anthropocene*, vol. 45. Elsevier Ltd, Mar. 01, 2024. https://doi.org/10.1016/j.ancene.2024.100427

[4] C. Masciopinto and I. S. Liso, "Assessment of the impact of sea-level rise due to climate change on coastal groundwater discharge," *Science of the Total Environment*, vol. 569–570, pp. 672–680, Nov. 2016, https://doi.org/10.1016/j.scitotenv.2016.06.183

[5] D. Caesario, K. Gisevius, E. Purwaningsih, D. Rachmawati, and B. Braun, "Characterization of Hydrogeological Parameters for Groundwater Resource Management in Coastal Urban Environments: Patenggangan Beach, Padang City, West Sumatra," in *IOP Conference Series: Earth and Environmental Science*, Institute of Physics, 2025. https://doi.org/10.1088/1755-1315/1547/1/012006

[6] J. F. Águila *et al.*, "Time-lapse resistivity imaging and self-potential monitoring of experimentally induced saline intrusion in coastal aquifer sands," *Science of the Total Environment*, vol. 972, Apr. 2025, https://doi.org/10.1016/j.scitotenv.2025.179104

[7] A. Hilmi, A. M. Ulfa, A. Wijaya, and L. I. Hadimi, "Study of seawater intrusion in coastal aquifer using total dissolved solid, conductivity and salinity measurement in Labuhan Kertasari Village, West Sumbawa," in *Journal of Physics: Conference Series*, IOP Publishing Ltd, Mar. 2021. https://doi.org/10.1088/1742-6596/1816/1/012064

[8] V. Charly, H. Hendrayana, and C. Nait, "Assessing the Impact of Seawater Intrusion on Groundwater Using Geo-indicators in Padang City," in *IOP Conference Series: Earth and Environmental Science*, Institute of Physics, 2025. https://doi.org/10.1088/1755-1315/1451/1/012002

[9] M. Chairi, W. Purba, W. Boy, R. Imani, and J. Melasari, "Shallow Well Water Salinity Viewed from Distance of Well to CoastLine and Ground Water Level Elevation in Purus Padang Village," in *Journal of Physics: Conference Series*, Institute of Physics Publishing, Dec. 2019. https://doi.org/10.1088/1742-6596/1339/1/012004

[10] N. Trabelsi, I. Triki, I. Hentati, and M. Zairi, "Aquifer vulnerability and seawater intrusion risk using GALDIT, GQISWI and GIS: case of a coastal aquifer in Tunisia," *Environ. Earth Sci.*, vol. 75, no. 8, Apr. 2016, https://doi.org/10.1007/s12665-016-5459-y

[11] E. Putriany and S. P. Sejati, "Preliminary study of sea water intrusion using geographic information system in Temon, Kulon Progo, Yogyakarta, Indonesia," *Jurnal Pendidikan Geografi: Kajian, Teori, dan Praktek dalam Bidang Pendidikan dan Ilmu Geografi*, vol. 28, no. 2, Apr. 2024, https://doi.org/10.17977/um017v28i22023p193-208

[12] M. Perumal, S. Sekar, and P. C. S. Carvalho, "Global Investigations of Seawater Intrusion (SWI) in Coastal Groundwaters in the Last Two Decades (2000–2020): A Bibliometric Analysis," *Sustainability (Switzerland)*, vol. 16, no. 3. Multidisciplinary Digital Publishing Institute (MDPI), Feb. 01, 2024. https://doi.org/10.3390/su16031266

[13] A. W. Hastuti, M. Nagai, N. P. Ismail, B. Priyono, K. I. Suniada, and A. Wijaya, "Spatiotemporal analysis of shoreline change trends and adaptation in Bali Province, Indonesia," *Reg. Stud. Mar. Sci.*, vol. 76, Dec. 2024, https://doi.org/10.1016/j.rsma.2024.103598

[14] A. M. Jibrin, M. Al-Suwaiyan, Z. M. Yaseen, and S. I. Abba, "New perspective on density-based spatial clustering of applications with noise for groundwater assessment," *J. Hydrol. (Amst).*, vol. 661, p. 133566, Nov. 2025, https://doi.org/10.1016/j.jhydrol.2025.133566

[15] Y. Wang *et al.*, "Integrating machine learning with spatial analysis for enhanced soil interpolation: Balancing accuracy and visualization," *Smart Agricultural Technology*, vol. 11, Aug. 2025, https://doi.org/10.1016/j.atech.2025.101032

[16] S. Saad, A. A. Javadi, R. Farmani, and M. Sherif, "Efficient uncertainty quantification for seawater intrusion prediction using Optimized sampling and Null Space Monte Carlo method," *J. Hydrol. (Amst).*, vol. 620, May 2023, https://doi.org/10.1016/j.jhydrol.2023.129496

[17] P. Tziachris *et al.*, "Spatial or Random Cross-Validation? The Effect of Resampling Methods in Predicting Groundwater Salinity with Machine Learning in Mediterranean Region," *Water (Switzerland)*, vol. 15, no. 12, Jun. 2023, https://doi.org/10.3390/w15122278

[18] A. Hilal *et al.*, "Geostatistical modeling—a tool for predictive soil mapping," in *Remote Sensing in Precision Agriculture*, Elsevier, 2024, pp. 389–418. https://doi.org/10.1016/B978-0-323-91068-2.00011-4

[19] P. Goovaerts, "Kriging and semivariogram deconvolution in the presence of irregular geographical units," *Math. Geosci.*, vol. 40, no. 1, pp. 101–128, 2008, https://doi.org/10.1007/s11004-007-9129-1

[20] D. M. K. Zebaze *et al.*, "Integrated geophysical, hydrochemical, and machine learning framework for sustainable groundwater management in West African coastal aquifers: Insights from Kribi, Cameroon," *J. Hydrol. Reg. Stud.*, vol. 62, Dec. 2025, https://doi.org/10.1016/j.ejrh.2025.102922

[21] M. Fardilla *et al.*, "Literature Review: Analysis of Coastal Vulnerability and Comprehensive Adaptation Strategies in Padang City, West Sumatra," *Zona Laut Jurnal Inovasi Sains Dan Teknologi Kelautan*, pp. 381–386, Nov. 2025, https://doi.org/10.62012/zl.vi.47591

[22] R. Guild, X. Wang, and P. A. Quijón, "Climate change impacts on coastal ecosystems," *Environmental Research: Climate*, vol. 3, no. 4. Institute of Physics, Dec. 01, 2024. https://doi.org/10.1088/2752-5295/ad9f90

[23] L. Belkhiri, A. Tiri, and L. Mouni, "Spatial distribution of the groundwater quality using kriging and Co-kriging interpolations," *Groundw. Sustain. Dev.*, vol. 11, p. 100473, Oct. 2020, https://doi.org/10.1016/j.gsd.2020.100473

[24] J. Wu, W. A. Norvell, and R. M. Welch, "Kriging on highly skewed data for DTPA-extractable soil Zn with auxiliary information for pH and organic carbon," *Geoderma*, vol. 134, no. 1–2, pp. 187–199, Sep. 2006, https://doi.org/10.1016/j.geoderma.2005.11.002

[25] M. Maleki, X. Emery, and N. Mery, "Indicator Variograms as an Aid for Geological Interpretation and Modeling of Ore Deposits," *Minerals*, vol. 7, no. 12, p. 241, Dec. 2017, https://doi.org/10.3390/min7120241

[26] P. K. Dash, B. A. Miller, N. Panigrahi, and A. Mishra, "Exploring the Effect of Sampling Density on Spatial Prediction with Spatial Interpolation of Multiple Soil Nutrients at a Regional Scale," *Land (Basel).*, vol. 13, no. 10, p. 1615, Oct. 2024, https://doi.org/10.3390/land13101615

[27] T. C. Maltauro, M. A. Uribe-Opazo, L. P. C. Guedes, M. Galea, and O. Nicolis, "Spatial–Temporal Variability of Soybean Yield Using Separable Covariance Structure," *Agriculture*, vol. 15, no. 11, p. 1199, May 2025, https://doi.org/10.3390/agriculture15111199

[28] S. Yu, L. Zhao, and S. Li, "Leveraging Deep Learning for Automated Experimental Semivariogram Fitting," *Atmosphere (Basel).*, vol. 16, no. 2, p. 191, Feb. 2025, https://doi.org/10.3390/atmos16020191

[29] H. Arslan, "Spatial and temporal mapping of groundwater salinity using ordinary kriging and indicator kriging: The case of Bafra Plain, Turkey," *Agric. Water Manag.*, vol. 113, pp. 57–63, Oct. 2012, https://doi.org/10.1016/j.agwat.2012.06.015

[30] Y. Yang, P. Ma, X. Hu, Y. Gao, and C. Wang, "Testing spatial interpolation methods for deep-time organic carbon burial in epicontinental seas by taking Sunda Shelf as an example," *Mar. Geol.*, vol. 486, p. 107566, Aug. 2025, https://doi.org/10.1016/j.margeo.2025.107566

[31] A. R. Samsudin, A. Haryono, U. Hamzah, and A. G. Rafek, "Salinity mapping of coastal groundwater aquifers using hydrogeochemical and geophysical methods: a case study from north Kelantan, Malaysia," *Environmental Geology*, vol. 55, no. 8, pp. 1737–1743, Oct. 2008, https://doi.org/10.1007/s00254-007-1124-9

[32] A. A. N., O. P. I., Y. J., O. E. A., N. H. O., and A. Y. B., "Geostatistical Assessment of Groundwater Quality from Coastal Aquifers of Eastern Niger Delta, Nigeria," *Journal of Geo-sciences*, vol. 2, no. 3, pp. 51–59, May 2012, https://doi.org/10.5923/j.geo.20120203.03

[33] M. A. Mujib, S. Astutik, B. Apriyanto, I. N. Muhammad, and A. A. Fitra, "Geostatistical Mapping of Groundwater Salinity and Seawater Intrusion in Coastal Aquifers of Jember Regency Using Physicochemical Parameters and Seawater Fraction," *Geomedia Majalah Ilmiah dan Informasi Kegeografian*, vol. 22, no. 2, pp. 196–212, Nov. 2024, https://doi.org/10.21831/gm.v22i2.77550

[34] G. B. M. Heuvelink and R. Webster, "Spatial statistics and soil mapping: A blossoming partnership under pressure," *Spat. Stat.*, vol. 50, p. 100639, Aug. 2022, https://doi.org/10.1016/j.spasta.2022.100639

[35] M. Manaf, Z. Ali, and M. Scholz, "Integrating random forest-based regression kriging for analyzing spatial variability of rainfall in arid and semi-arid regions," *Sci. Rep.*, vol. 16, no. 1, p. 5298, Jan. 2026, https://doi.org/10.1038/s41598-026-36074-4

[36] A. El-Azhari *et al.*, "Evaluating groundwater salinity patterns and spatiotemporal dynamics in complex endorheic aquifer systems," *Science of The Total Environment*, vol. 994, p. 180055, Sep. 2025, https://doi.org/10.1016/j.scitotenv.2025.180055

[37] G. SAHBENİ and B. SZÉKELY, "Spatial modeling of soil salinity using kriging interpolation techniques: A study case in the Great Hungarian Plain," *EURASIAN JOURNAL OF SOIL SCIENCE (EJSS)*, vol. 11, no. 2, pp. 102–112, Apr. 2022, https://doi.org/10.18393/ejss.1013432

[38] Y. Wijayanto, M. A. D. Kustianto, S. A. Budiman, and I. Purnamasari, "Using Geostatistics for Spatial Analysis of Soil Moisture Content, Electrical Conductivity, and pH at Paddy Fields," *JOURNAL OF TROPICAL SOILS*, vol. 28, no. 2, pp. 47–56, Nov. 2022, https://doi.org/10.5400/jts.2023.v28i2.47-56

[39] V. Charly, H. Hendrayana, and C. Nait, "Assessing the Impact of Seawater Intrusion on Groundwater Using Geo-indicators in Padang City," *IOP Conf. Ser. Earth Environ. Sci.*, vol. 1451, no. 1, p. 012002, Feb. 2025, https://doi.org/10.1088/1755-1315/1451/1/012002

Nomenclature

$\gamma(h)$	:	Semivariance at lag distance h Squared unit of variable
$\hat{\gamma}(h)$	:	Empirical semivariance at lag distance h Squared unit of variable
h	:	Separation distance between two observation points m
si	:	Spatial location of observation point i Coordinate
sj	:	Spatial location of observation point j Coordinate
Z(si)	:	Measured variable value at location si pH, µS/cm, mg/L, ppt
N(h)	:	Number of point pairs within distance class h
C0	:	Nugget effect Squared unit of variable
C	:	Partial sill (structured variance component) Squared unit of variable
C0 + C	:	Total sill Squared unit of variable
a	:	Range parameter m
α	:	Practical range m
λi	:	Kriging weight for observation i
µ	:	Lagrange multiplier in Ordinary Kriging
Z*(s0)	:	Predicted value at unsampled location s0 pH, µS/cm, mg/L, ppt
$\sigma k^2(s0)$	:	Kriging variance at location s0 Squared unit of variable
ei	:	Residual in cross-validation Same as variable
ME	:	Mean Error Same as variable
RMSE	:	Root Mean Square Error Same as variable
RMSSE	:	Root Mean Square Standardized Error
R^2	:	Coefficient of determination
OK	:	Ordinary Kriging
LOOCV	:	Leave-One-Out Cross-Validation
EC	:	Electrical Conductivity µS/cm
TDS	:	Total Dissolved Solids mg/L
pH	:	Potential of Hydrogen
Salinity	:	Salinity ppt
UTM	:	Universal Transverse Mercator
WGS 84	:	World Geodetic System 1984